

# From sintering to particle discrimination: New opportunities in Metal-Organic Frameworks scintillators

Vincent Villemot, Nicolas Dufour, Sharvanee Mauree, Benoit Sabot, Guillaume Bertrand, Matthieu Hamel

▶ **To cite this version:**

Vincent Villemot, Nicolas Dufour, Sharvanee Mauree, Benoit Sabot, Guillaume Bertrand, et al.. From sintering to particle discrimination: New opportunities in Metal-Organic Frameworks scintillators. Advanced Photonics Research, 2021, pp.2100259. 10.1002/adpr.202100259 . cea-03442303

**HAL Id: cea-03442303**
**https://cea.hal.science/cea-03442303**

Submitted on 23 Nov 2021

**HAL** is a multi-disciplinary open access archive for the deposit and dissemination of scientific research documents, whether they are published or not. The documents may come from teaching and research institutions in France or abroad, or from public or private research centers.

L'archive ouverte pluridisciplinaire **HAL**, est destinée au dépôt et à la diffusion de documents scientifiques de niveau recherche, publiés ou non, émanant des établissements d'enseignement et de recherche français ou étrangers, des laboratoires publics ou privés.



Distributed under a Creative Commons Attribution 4.0 International License

# From sintering to particle discrimination: New opportunities in Metal-Organic Frameworks scintillators

*Vincent Villemot, Nicolas Dufour, Sharvanee Mauree, Benoît Sabot, Guillaume H. V. Bertrand, Matthieu Hamel*

V. Villemot*, N. Dufour, S. Mauree, Dr. B. Sabot, Dr. G. H. V. Bertrand, Dr. M. Hamel*
Université Paris Saclay, CEA, List, F-91120 Palaiseau, France.
vincent.villemot@cea.fr and matthieu.hamel@cea.fr
Orcid numbers: 0000-0002-9478-6651 (VV), 0000-0001-8551-709X (ND), 0000-0003-3043-8006 (BS), 0000-0003-2061-9241 (GHVB), 0000-0002-3499-3966 (MH).

Keywords: MOF, scintillator, densification, photoluminescence, radioluminescence, MCNP, discrimination

Abstract:

The characterization of a scintillating Metal Organic Framework (MOF) is not straightforward, mainly due to the small size and low density of the material. In this context, we present herein a generic method to give an easy access to the determination of a key parameter in the scintillation field, namely the light output. To reach this, MOF-205 was first synthesized as millimetric-size single crystals then sintered under pressure and temperature conditions to afford a pellet. The density was increased by 300% while maintaining optical properties on par with scintillation application. The as-prepared scintillator was then characterized in terms of photoluminescence (UV-excited emission spectrum, time-correlated single photon counting) and radioluminescence spectroscopy (beta-excited emission spectrum, alpha, beta and gamma pulse height spectra, alpha/beta and alpha/gamma discrimination). Results were compared with commercial BC-404 plastic scintillator performances as well as supported by MCNP6.2 simulation.

## 1. Introduction

Methods to detect, qualify and quantify ionizing radiations were introduced soon after the discovery of radioactivity by Henri Becquerel in 1896. Currently, numerous applications benefit from this field, ranging from nuclear activities, research in high-energy physics, astronomy,

homeland security and medicine. Depending on the radionuclide to be detected, various disintegrations can occur, the most common and probable leading to the emission of alpha or beta particles often followed by de-emissions producing X and/or gamma rays. These ionizing radiations can be detected with scintillators, which are materials that are efficient to produce light when exposed to such radiations. This specific class of photoluminescent materials is divided into two main categories, namely inorganic and organic scintillators.[1] The former subclass appeared as early as 1895 (barium tetracyanoplatinate(II) $BaPt(CN)_4$[2]). The later was pioneered when the use of naphthalene was first reported in 1947.[3] Since these seminal publications, many efforts have been performed in the two chemistry worlds for the quest of the 'best' scintillator. However, both have pros and cons and currently no photoluminescent material represents the Holy Grail that could fulfil all requirement in terms of radiation detection (among others: detection efficiency against production cost). In this context, scientists have considered using advantages from both worlds, hence leading to a various range of scintillators such as sol-gel, hybrid materials or nanoparticles-loaded plastics.[4] Most particularly, composite scintillators stand out as they can bypass a lot of limitations. The core idea is to take a known efficient scintillator, mainly an organic or inorganic single crystal, and embed them into a matrix of suitable polymer. This will give access to what can be described as a polycrystalline scintillator. As single crystals are often hard to produce in large scale or are not very stable towards ambient condition (mechanical weakness, humidity and temperature dependency), this technology affords a way to combine large quantity of efficient scintillator and stability-aimed encapsulation.

Metal organic frameworks (MOFs) are a class of hybrid materials.[5] Under their crystalline form, they have found great interest to many researchers in a wide variety of fields because of their great versatility.[6] They are constructed of inorganic nodes linked with each other by organic ligands. Therefore, the modification of one or both bricks allows modifying the final properties, the only limitation being thus the creativity of the scientist. Allendorf *et al.* were the

first to highlight the possibility to use MOFs as potent scintillators. They observed decent light outputs (up to 22% of anthracene, ca. 3,300 ph·MeV$^{-1}$) by switching traditional organic linkers for a dicarboxylated *trans*-stilbene, an already known and efficient scintillating molecule.[7] Thanks to the above mentioned high degree of versatility of MOF construction, some researchers, again using ligands based on scintillating molecules, have also assembled frameworks based on traditional inorganic bricks and heavier metals to increase the stopping power of X-rays. For example, Wang *et al.* have synthesized two different 9,10-di(*para*-carboxyphenyl)anthracene (DPA)-based MOFs,[8] where one was connected to Zr nodes whereas the other to Hf nodes. As the two materials have different X-ray cross sections, it was possible to show a qualitative increased sensitivity for Hf-MOF.

Recently, new contributions have emerged involving Metal-Organic Frameworks as scintillators, having in mind their use in medical applications such as TOF-PET detectors.[9] Perego *et al.* have embedded the DPA-based Zr-MOF (previously synthesized by Wang[8]) inside two polymeric matrices: poly(dimethylsiloxane) (PDMS) and poly(methyl methacrylate) (PMMA). As MOFs can be hard to synthesize in large crystals, difficult to scale up and tricky to handle, composite materials seem to be the go-to solution to test them as scintillators. However, several limitations are foreseen with the incorporation of a MOF inside a matrix, and in general to the characterization of MOFs as scintillators. Despite efforts by chemists to synthesize MOF nanocrystals, these are subject to strong light scattering already at a low percentage of incorporation in the polymer matrix, which can lead to turbidity observed at loading as low as 0.5 weight%. This is mainly cause by the incorrect matching between the matrix and MOFs refractive index which lead to light scattering. This effect coupled to the numerous interfaces between the matrix and the embedded MOF can thus lead to strong deviation from the optimal light collection. These cumulated factors are altering the global optical properties and leading to a moderate scintillating material (6% the light output of anthracene, which is ca. 1,000 ph·MeV$^{-1}$). Other literature from this field generally describes

analytical methods that have to be adapted to small-size and low-density MOF materials, for example with Ion Beam Induced Luminescence[7] (IBIL) or small X-ray tubes,[8]. This experiments require high dose delivery[8, 9] or tedious characterization in liquid suspension.[8] Such techniques are useful but developing a universal characterization method for scintillating MOFs the closest to their final use, which means confronted to the presence of radionuclides and without form factor (e.g. single crystals dispersed in a liquid) would be of great value for the scientific community, and that was the core idea at the root of this study.

To overcome these issues, this work presents two major contributions leading to scintillating materials made from MOFs. The first concerns the densification by sintering until translucent media are reached.[10] The second concerns the nearly transparent pellet entirely composed by a luminescent MOF, and its use as scintillator. This application becomes particularly natural and of practical use to determine one of the scintillator key parameter: the light output. Experimental results, validated by particle radiation transport simulations performed with the MCNP6.2 Monte Carlo code allowed for the first time to characterize a Metal Organic Framework under alpha, beta and gamma excitation, and to observe a light output that can compete with a commercial plastic scintillator (BC-404, Saint-Gobain Crystals and Detectors[).[11,12] . Furthermore the hybrid nature of our sintered MOF was put in the perspective of classical inorganic and organic crystal scintillation. Those fields are known to demonstrate good particle discrimination by PSD. This approach was applied to our materials and unprecedented particle discrimination with scintillating MOFs has been reached, confirming precedent hint from Allendorf *et al*.[15]

## 2. Results and discussion

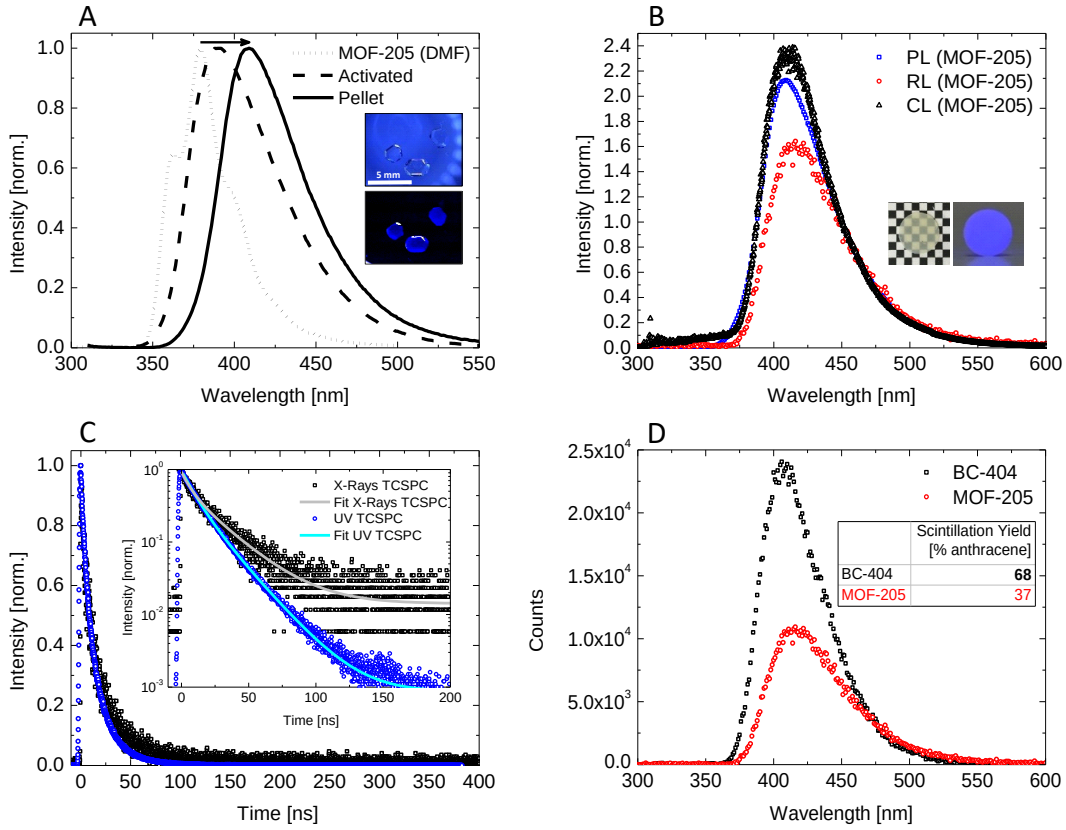



**Figure 1.** Structural and photophysical properties of sintered MOF-205. A) Photoluminescence spectra of MOF-205 in DMF (dotted line), activated (dashed line) and pellet (solid line). Inset are pictures of millimetric single crystals under visible light and under 365 nm excitation light. B) Normalized steady-state Photoluminescence (PL), Radioluminescence (RL) and Cathodoluminescence (CL) spectra of sintered MOF-205. Inset are pictures of pellet under visible light and under 365 nm excitation light (excitation source was placed behind the pellet). C) Time-Correlated Single Photon Counting (TCSPC) of sintered MOF-205 after 274 nm excitation (blue) and X-rays excitation (black). Decay values are the result of a biexponential fitting with a $R^2 = 0.99$. D) Radioluminescence spectra of BC-404 and MOF-205 (both are ⌀ 13 mm and thickness 400 µm). Area integration allows to recover the scintillation efficiency values.

As demonstrated in many contributions, MOF synthesis is tricky and requires attention as an impurity can have a large impact on the final photophysical properties.[13] As a case study, we chose a MOF where the secondary building unit is $Zn_4O$, linked with two different organic linkers: 1,3,5-tris(4-carboxyphenyl)benzene ($H_3BTB$) and 2,6-naphthalene dicarboxylate (2,6-NDC), which is also named MOF-205 or DUT-6.[14,15] It was selected as a potent candidate thanks to its photoluminescent properties that comply with standard plastic scintillators: fast decay time and emission wavelength centered around 420 nm. These interesting features are

carry by the naphthalene moiety, which is a well-known molecule in the scintillation field.[16] The second reason is that this framework presents a cubic lattice structure, which is compliant with sintering application, a key in densification. Theoretically, under uniaxial pressure planes of cubic structures should move isotropically and finally result in a material densification, a result that would be less easy to achieve with non-cubic lattices[10], or anisotropic collapses. Here we propose a densification of MOF under two external stimuli: pressure and temperature. This has already been demonstrated by Zacharia *et al.* only under the action of pressure for MOF-177, a MOF that is similar to MOF-205.[17] This trend remains marginal as the purpose of synthesizing MOF is, classically, to use their porosity properties, which is not compatible with densification.

Thus, MOF-205 was synthesized to obtain large, pure, millimeter-sized crystals (Inset of **Figure 1.A**), was sintered and fully characterized (see Supporting Information, Figure S1). As heat can promote the plastic displacement leading to densification, temperature limits should be defined in order to prevent any parasitic degradation of the (photo)physical properties. Thus, thermal decomposition behavior was investigated in order to characterize its thermal stability. As shown in Figure S2, thermogravimetric analysis (TGA) shows two characteristic weight losses. The first continuous weight loss of 9.9% in the temperature range from 30 °C to 350 °C corresponds to the desorption of guest molecules. The second drastic loss of 66.4% occurring at 450 °C corresponds to the decomposition of the frameworks to ZnO and organic byproduct. From this analysis, we decided to constrain the sintering to an operating window between 30 °C and 200 °C in order to avoid any deterioration of the MOF during this process. Thus, activated powder of MOF-205 was pressed under 15 tons in a 13 mm diameter dye at 100 °C for 20 min, corresponding to a pressure of 1.1 GPa. The resulting pellet (Inset of **Figure 1.B**) presented a thickness of 400 ± 20 µm and a mass of 82 mg. Considering the pellet as a perfect cylinder, a density of $1.56 \pm 0.08$ was calculated, which represents a remarkable increase of 300% compared to its original density (0.38).[14] Furthermore, the resulting pellet displayed promising

photophysical properties. Main spectral characteristics were obtained from either UV photluminescence (PL) or ionizing radiation such as radioluminescence (RL) with an $^{90}Sr/^{90}Y$ beta source or cathodoluminescence (CL) with an X-ray excitation. The results are shown in **Figure 1.A-D**, and discuss below.

At the origin of our composite scintillator, MOF-205 in DMF presents an emission of 380 nm with characteristic vibronic structure of linker in its dilute form (**Figure 1.A**). This is characteristic of a ligand-centered emission. As already mentioned in many publications, frameworks are likely to be dependent on their environment, guest molecules or impurities trapped inside their porosity. Fluorescence is especially sensitive to external stimuli when it arises from the linker only as is the case for MOF-5 for example.[18] Hence, upon activation the material looses its fine structure and shows a Gaussian-type emission centered at higher wavelengths (394 nm). Then after pressing, the pellet shows a slightly different steady-state photoluminescence as the fluorescence maximum undergoes a shift to 409 nm (**Figure 1.B**). This wavelength increase could be explained by larger π overlaps between the ligands due to the densification of the material and the reduction of the ligands distance to each other. Thus, the energy gap would be reduced and would result in a bathochromic shift at the image of the ligand in its solid form ($\lambda_{em}$ = 452 nm) (Figure S3). This assumption is confirmed by a comparison of the time-resolved fluorescence spectra. Under the effect of pressure and temperature the material therefore tends to amorphise and favours a spatial rearrangement of the ligands which leads to emission at a higher wavelength. This is confirmed as the pellet shows no X-ray diffraction. This trend is as also demonstrated by Zacharia et *al.* for a similar MOF.[17] However, we assume that this structural change remains minor as the average lifetime is only slightly changed compared to pure activated MOF-205 single crystal (Figure S4). This results collectively show that MOF-205 as a single crystal or sintered as a pellet have the same photophysical behavior. Sintered pellets are hence a good sudo-sample to judge the scintillation

response of a MOF. Pellets are also more practical to use andstarting from this point, we are considering the pellets as scintillating material in their own rights.

Radioluminescence (RL) and cathodoluminescence (CL), contrary to PL, allow the investigation of excited states by ionization with radionuclides. As known, ionization process is quite different from PL as ionization can lead to several changes in the electronic and molecular structure of matter, thus expectable discrepancies in emission wavelength or/and in lifetime. **Figure 1.B** compares normalized PL, RL and CL state spectra. Since RL and CL/PL are recorded in transmission and front face, respectively, it is possible to notice several changes in the shape of the Gaussian-type emission. This is mainly due to reabsorption and diffusion occurring within the pellet. However, since traditional scintillation measurements are usually performed in transmission, the RL experiment is closer to the application measurement method. **Figure 1.C** represents the Time-Correlated Single Photon Counting (TCSPC) of sintered MOF-205 after 274 nm excitation (blue) and X-rays excitation (black). It is interesting to note that under X-rays excitation the pellet shows a fast and slow component in similar magnitudes as under UV excitation. However, the weights of each components are different. Thus, the average lifetime increases from 14.8 to 17.8 ns (Figure S5). This could be explained by a larger population.

To highlight the use of sintered pellet of MOF-205, RL measurements were carried out with a well-known reference in the scintillation field, namely BC-404 (Saint-Gobain Crystals and Detectors) with same size and shape: a cylinder with 13 mm diameter and 400 µm thickness. Both materials can thus be compared, provided that the experimental set up is identical as well. This is shown in a radioluminescence experiments presented in **Figure 1.D**. As the area under the curve corresponds to the amount of emitted photons, it is possible to estimate a scintillation efficiency by a rule of thumb. MOF-205 emits 55% of what the BC-404 is capable. In other words, this means that MOF-205 has a light output of 37% compared to anthracene, as the BC-

404 is 68% according to its datasheet.[11] Considering that anthracene is ≈ 15,000 ph·MeV$^{-1}$, the light output of the sintered MOF-205 is thus around 5,500 ph·MeV$^{-1}$. The above results validate the concept of a sintered MOF-205 as an intrinsic scintillator and places it above other MOF-based scintillators as far as light output is concerned.

As the pellets are quite thin, the use of alpha-emitting source is obvious in terms of characterization with radionuclides. Alpha emitters have a short penetration distance in matter, and therefore ionize the pellet by depositing all their energy as shown by simulation (Inset of **Figure 2.A**). For instance, the alpha emitter $^{244}$Cm presents two characteristics energy lines at 5.804 MeV (76.7%) and 5.762 MeV (23.3%).[19] With this energy, alpha particles from $^{244}$Cm are fully stopped within 400 µm of both scintillators, as it was confirmed by MCNP6.2 simulation. The maximum interaction depth was simulated at 37 µm and 45 µm for MOF-205 and BC-404, respectively. We explain this interaction depth difference from the MOF-205 higher density. Due to the detector's resolution and small energy difference between the two alpha rays, it is expected that a single Gaussian-like spectra would be observed. In addition, considering large ionization quenching that are classically encountered with alpha emitters in plastic scintillators (12% of total energy), we expect to see the full absorption peak of the $^{244}$Cm alphas around 560 keV.[20] Results in **Figure 2.A** show that both BC-404 and MOF-205 present a full absorption of $^{244}$Cm at channels 18500 and 6500, respectively. However, the light output of the latter was quantified and estimated at 57% the one of BC-404, hence the Gaussian mean value should be expected at higher channel value (≈ 10,000). One hypothesis is the loss of photons due to scattering in the MOFs, which is not as transparent as BC-404 plastic scintillator. This was verified by measuring a pellet twice the width. The blue curve of an 800 µm thin MOF-205 in **Figure 2.A** shows that the Gaussian peak is very close to the photomultiplier tube noise, thus highlighting the importance of transparency. This is combined with the higher stopping power of MOF-205 as was mentioned before, thus leading to an even more localized interaction (ionization quenching), magnifying the light loss by self-quenching and increasing

the pathway for photon transport within this material. To confirm this hypothesis, beta acquisitions were carried out.

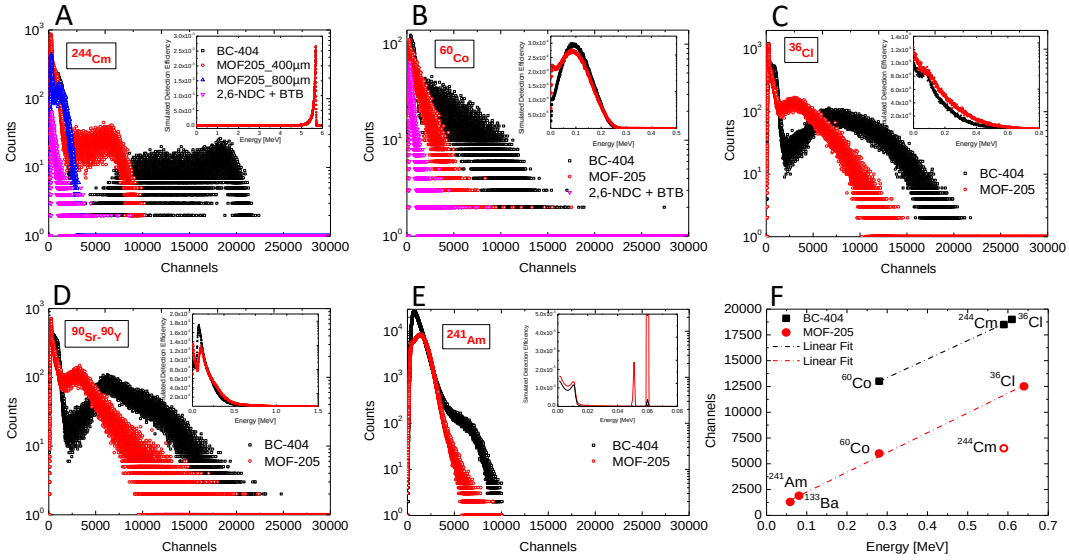



**Figure 2. Comparison between scintillation performances of MOF-205 and BC-404.** Histogram of scintillation data for BC-404 (black), MOF-205_400µm (red), MOF-205_800 µm (blue) and 2,6-NDC/BTB in stoichiometric quantity (pink) in presence of **A)** $^{244}$Cm, **B)** $^{60}$Co, **C)** $^{36}$Cl and **D**) $^{90}$Sr-$^{90}$Y. **E)** $^{241}$Am pulse coincidence spectra. Inset in each graph represents the simulated pulse height spectrum. **F)** Channel position of the scintillators' response versus impinging energy.

Beta emission spectra are continuous and beta particles present deeper tracks in the matter than alpha particles, resulting in full or partial energy deposition in the detector, depending of the incident energy. Three beta radionuclides were used in this study with their main emission as follows: $^{60}$Co ( $E_\beta^{mean}$ = 95 keV, $E_\beta^{max}$ = 317 keV), $^{36}$Cl ( $E_\beta^{mean}$ = 316 keV, $E_\beta^{max}$ = 709 keV) and $^{90}$Sr/$^{90}$Y ( $E_\beta^{mean}$ = 196 keV, $E_\beta^{max}$ = 546 keV for $^{90}$Sr, $E_\beta^{mean}$ = 927 keV, $E_\beta^{max}$ = 2279 keV for $^{90}$Y).[19] Experimental beta acquisition for both BC-404 and MOF-205 are represented in **Figure 2.B-D** with their respective simulated detection efficiency. MCNP6.2 simulation stops at the particle-matter interaction and energy deposition, so do not simulate any luminescence phenomenon nor any light propagation. Therefore, similar simulation spectra may lead to different experimental spectra, with discrepancies originating from light generation and propagation. As shown, going from low-energy emitter $^{60}$Co to a

higher energy emitter $^{36}Cl$ led to an increasing response in channels, thus in deposited energy. However, comparing $^{36}Cl$ spectrum with a much higher energy emitter such as $^{90}Sr/^{90}Y$, no important change of the spectrum was noticed. This is not surprising considering the high-energy $^{90}Sr$ beta particles compared to the size of the pellet. Simulated detection efficiency (Inset of **Figure 2.D**) confirms that the generation of less photons comes therefore from a partial energy deposition within the pellet, as both energy deposition spectra are similar in shape and intensity.

Moving on to gamma detection possibility, and knowing that the geometry of our scintillators is not ideal for such detection (which requires large detector volume in general), several scintillation spectra were recorded using low-energy gamma emitter such as $^{241}Am$ ($E_\gamma$ = 59.5 keV (36.9%), **Figure 2.E**) and $^{133}Ba$ ($E_\gamma$ = 81 keV (33.3 %) and 356 keV (62.0 %), Figure S6), and compared to simulation. To avoid the possible $^{241}Am$ alpha interaction, a thin layer of paper was placed between the source and the detector. Simulation shows (Inset of **Figure 2.E**) a noticeable 59.5 keV full absorption peak (PE) that is observable only for MOF-205 due to its higher density than BC-404. Experimentally, this was partially confirmed as BC-404 and MOF-205 spectra showed scintillation response discrepancies. BC-404 is composed of a Compton edge (CE) whereas MOF-205 is composed of a unique Gaussian-type spectrum. We expect that it is a convolution of CE and PE with the corresponding maximum attributed to the 59 keV gamma ray. As the considered energy is low and therefore near to the background noise, we used a coincidence assembly to go deeper in our interpretation. Comparison between forms of both spectra (Figure S7) also shows discrepancy. The fact that there are two patterns for MOF-205 is in agreement with our above explanation. So far, the best explanation is that due to the poor resolution of our measurement chain, it is not possible to correctly separate the Compton edge from the PE. Instead, we have a convolution of both corresponding distributions. This trend was also observed for $^{133}Ba$ (Figure S8). Contrary to the $^{241}Am$ configuration it is possible to distinguish two contributions. We hypothesized a probable 356 keV full absorption

peak but it was difficult to investigate and no formal conclusion was drawn even after 10 million pulses recorded. We estimate that the first visible maximum around channels 1900 corresponds to the 81 keV full absorption peak. By comparing the channels between $^{241}$Am and $^{133}$Ba, these contributions seem to correspond to the two emitted gamma at 81 keV and 356 keV confirming the above hypothesis. To the best of our knowledge, the observation of PE in MOF was never achieved yet and we believe that this was possible in this study due to increased densification.

Considering both simulation and experimental data, it was possible to establish a calibration curve by making a parallel with $^{244}$Cm alpha spectrum, $^{60}$Co and $^{36}$Cl beta emitters and gamma emitter such as $^{241}$Am and $^{133}$Ba. To do so, an energy deposition endpoint for beta distributions was read as the mean value between the first value that reaches zero and the last. For the specific alpha emitter $^{244}$Cm, the point was read as the average mean value of the peak. For $^{241}$Am and $^{133}$Ba gamma emitters, the point was taken into account only for MOF-205 as it presents a full absorption peak and it was read at the maximum of the curve endorsed by simulation. **Figure 2.F** shows the channels versus the corresponding simulated maximum energy deposition for BC-404 and sintered MOF-205. For BC-404, it is possible to say with confidence that our model fits well as the trend curve passes through the three points with an $R^2$ factor of 0.9998. This furthers confirms our beta endpoint determination method, which has sufficient precision for an energy calibration curve. Regarding MOF-205 the model looks consistent with the exception of $^{244}$Cm. This confirms the previous hypothesis that the auto-quenching for alpha ionization is more important in the MOF than within the BC-404, which means that the output energy is lower than the would be perceived 560 keV. It is also important to note that the trend is linear, even at low energy. However, it is well known that both organic and inorganic scintillator are not linear with the incident energy, this effect appearing below 100 keV.[21] This observation remains far beyond the scope of this study as the MOF scintillation is still a new field and requires further exploration to draw consistent conclusions.

Having explored the scintillation performances of the sintered MOF-205, we tried to challenge the material up a bit with the study of its potential discrimination properties. In particular, alpha/beta and alpha/gamma discrimination were evaluated. It is noteworthy that such properties are not straightforward for all-purpose scintillators and have never been studied in MOF scintillation to the best of our knowledge, even if it was hinted by previous results.[15] This discrimination is related to higher ionization densities within the material when the incoming particle becomes heavier. This lead to a denser population of excited state, causing increase proximity of triplet state. .[22] With two neighboring triplet states, annihilation may occur, thus leading to delayed fluorescence paving the way to discrimination between particles of different dE/dx.[23] MOFs belong to the class of supramolecules that are keen to perform triplet-triplet annihilation,[24] thus particle discrimination should be effective if properly recorded.

As mentioned, two case studies were performed with the same BC-404 and MOF-205 pellets. First is the alpha/beta discrimination, second is the alpha/gamma discrimination. Due to the small size of the MOF-205 scintillator compared with our 2.5 cm diameter sources, experiments were performed sequentially, that is to say alpha then beta or gamma spectra. **Figure 3, top** shows the bidimensional spectra of $^{244}$Cm (left), $^{36}$Cl (center) and their addition (right). Since the tail of alpha-related pulses is slightly longer than beta- or gamma-related pulses, the integration of the delayed charge over the total charge allows sorting the nature of the excitation that led to scintillation. Such pellet configuration is favorable for this discrimination as the scintillator is intrinsically poorly sensitive to gamma rays and alpha emitters see the full absorption of their energy within the material. But still and as expected, alpha/gamma discrimination using a gamma-emitting $^{133}$Ba source was also possible (**Figure 3, middle**). As a visual comparison, alpha/beta discrimination of BC-404 was less pronounced (**Figure 3, bottom**), with the two lobes being tilted with a positive slope for an unknown reason. BC-400, a close equivalent to BC-404 was found to display moderate α/β discrimination as well.[25]. In

addition, a noticeable Figure of Merit (FOM) of 0.55 was calculated over the full spectrum for both α/β and α/γ discrimination (Figure S9). Ultimately, fast neutron/gamma discrimination with MOF-205 was also tested but the results were harsh to interpret, mainly due to the small size of the material.

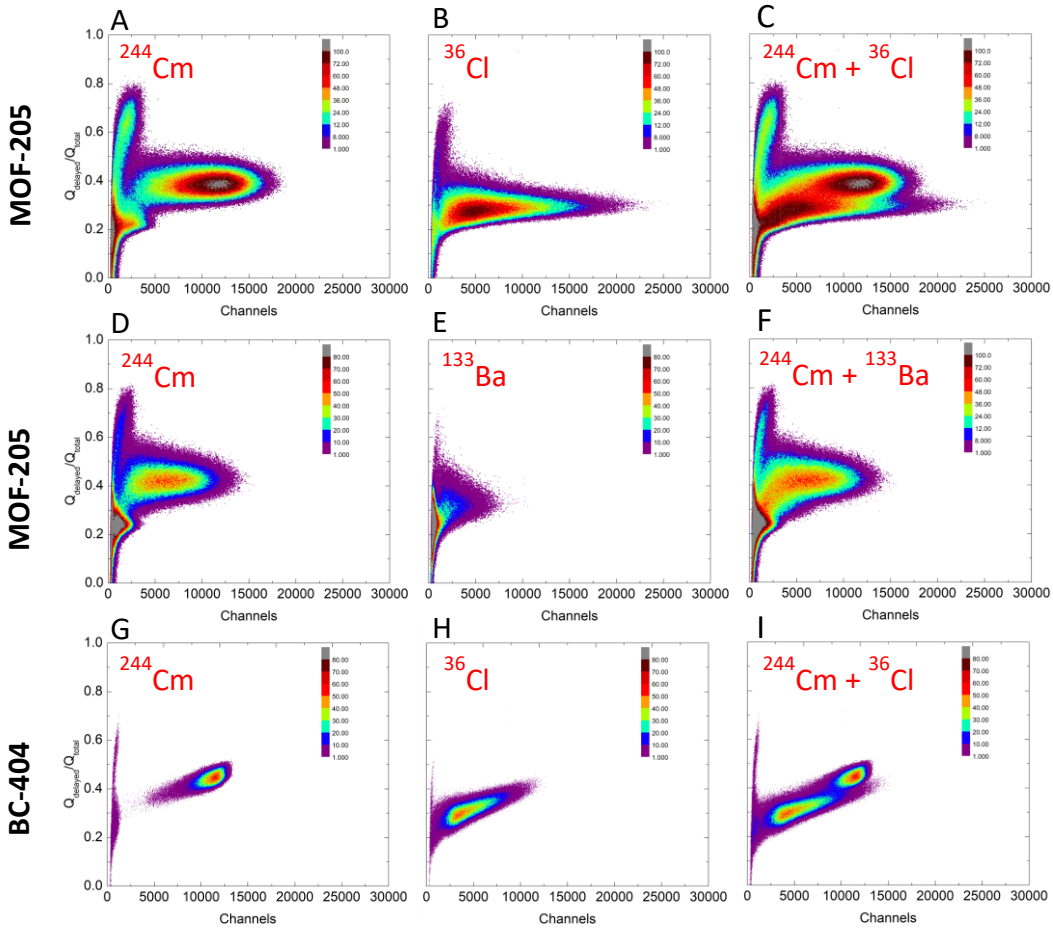



**Figure 3.** Pulse Discrimination spectra for various configurations. Left: $^{244}$Cm. Center: $^{36}$Cl or $^{133}$Ba. Right: superposition of the two precedent spectra. Note that the two $^{244}$Cm spectra for MOF-205 are not identical due to differences in the positioning of the source against the scintillator. See supporting information for full details.

## 3. Conclusion

In conclusion, an important advancement in scintillating MOFs characterization is presented here. Thanks to sintering process, the access to a key parameter such as the light output is now straightforward if one uses the most appropriate radionuclide (which means alpha or beta emitters) as the excitation. Here we recommend the use of $^{60}$Co or $^{36}$Cl as beta source, since

their energy is fully absorbed by the material and the stopping range is not too elevated. Thus, a 400 µm thick MOF-205 pellet displayed interesting scintillation properties, an emission wavelength of 409 nm, a mean decay time of 14.3 ns and a scintillation yield 37% the one of anthracene. Both alpha, beta and gamma experimental spectra were supported by MCNP6.2 calculations. Our sintered MOF was not fully transparent but the as-prepared pellet was prepared exclusively from MOF-205, as this was our main goal. Pellets potentially prepared with diluted MOF-205 with cubic powder of the same refractive index would lead to materials with better transparency. It is the first time that alpha/beta and alpha/gamma discrimination is qualitatively acknowledged for a MOF. Finally, this study opens a new and exciting research topic. First, we guess that sintered transparent MOFs, achieved for the first time in this work, will be an ongoing and explored field in the next years for optical application mainly. Secondly, this derivative class of metal organic frameworks constitutes a brand new class of scintillator full of opportunities. For instance by using the unique versatility of MOFs and by playing on the composition with heavy metal as nodes and on sintering parameters, we guess that it should be possible to be more sensitive to some ionization and therefore increase the energy response. The goal is to be positioned between organic and inorganic scintillators as a new class of hybrid materials. We hope that this report will be a tremendous input in the field as it brings two new concept relative to the already rich area of MOF: sintering and scintillation discrimination.

## Supporting Information

Supporting Information is available from the Wiley Online Library or from the author.

## Acknowledgements

The Authors wish to thank Pr. Christophe Dujardin for X-ray TCSPC measurement. This project has received funding from the European Union's Horizon 2020 research and innovation programme under Grant Agreement No 899293. This document reflects only the authors' view and the Commission is not responsible for any use that may be made or the information it contains

Received: ((will be filled in by the editorial staff))
Revised: ((will be filled in by the editorial staff))
Published online: ((will be filled in by the editorial staff))

385 References

[1] a) C. Dujardin, M. Hamel, in *Plastic Scintillators: Chemistry and Applications* (Ed: M. Hamel), Springer-Nature Switzerland AG, **2021**, Ch. 1, pp. 3-33. ; b) G. H. V. Bertrand, M. Hamel, F. Sguerra, *Chem. – Eur. J.* **2014**, *20*, 15660-15685.

[2] W. C. Röntgen, *Science* **1896**, *3*, 227.

[3] I. Broser, H. Kallmann, *Z. Naturforsch.* **1947**, *2a*, 642-650.

[4] a) M. Koshimizu, *Funct. Mater. Lett.* **2020**, *13*, 2030003; b) M. Koshimizu, in *Plastic Scintillators: Chemistry and Applications* (Ed: M. Hamel), Springer-Nature Switzerland AG, **2021**, Ch. 6, pp. 201-222.

[5] a) O. M. Yaghi, M. O'Keeffe, N. W. Ockwig, H. K. Chae, M. Eddaoudi, J. Kim, *Nature* **2003**, *423*, 705-714; b) G. Ferey, *Chem. Soc. Rev*. **2008**, *37*, 191-214.

[6] a) L. E. Kreno, K. Leong, O. K. Farha, M.D Allendorf, R. P. Van Duyne, J. T. Hupp *Chemical Reviews* **2012**, *112*(2), 1105-1125; b) W. P. Lustig, S. Mukherjee, N. D. Rudd, A. V. Desai, J. Li, S. K. Ghosh, *Chem. Soc. Rev*. **2017**, *46*, 3242-3285

[7] a) C. A. Bauer, T. V. Timofeeva, T. B. Settersten, B. D. Patterson, V. H. Liu, B. A. Simmons, M. D. Allendorf, *J. Am. Chem. Soc*. **2007**, *129*, 7136-7144; b) F. P. Doty, C. A. Bauer, A. J. Skulan, P. G. Grant, M. D. Allendorf, *Adv. Mater.* **2009**, *21*, 95-101; c) P. L. Feng, J. V. Branson, K. Hattar, G. Vizkelethy, M. D. Allendorf, F. P. Doty, *Nucl. Instr. Methods A* **2011**, *652*, 295-298; d) S. R. Mathis II, S. T. Golafale, J. Bacsa, A. Steiner, C. W. Ingram, F. P. Doty, E. Auden, K. Hattar, *Dalton Trans.*, **2017**, *46*, 491-500; e) S. R. Mathis II, S. T. Golafale, K. M. Solntsev, C. W. Ingram, *Crystals* **2018**, *8*, 53.

[8] C. Wang, O. Volotskova, K. Lu, M. Ahmad, C. Sun, L. Xing, W. Lin, *J. Am. Chem. Soc.*, **2014**, *136*, 6171-6174.

[9] J. Perego, I. Villa, A. Pedrini, E. C. Padovani, R. Crapanzano, A. Vedda, C. Dujardin, C. X. Bezuidenhout, S. Bracco, P. E. Sozzani, A. Comotti, L. Gironi, M. Beretta, M. Salomoni, N. Kratochwil, S. Gundacker, E. Auffray, F. Meinardi, A. Monguzzi, *Nat. Photonics* **2021**, *15*, 393-400.

[10] S. Grasso, M. Biesuz, L. Zoli, G. Taveri, A. I. Duff, D. Ke, A. Jiang, M. J. Reece, *Adv. Appl. Ceram.* **2020**, *119*, 115-143.

[11] C. J. Werner, J. S. Bull, C. J. Solomon, F. B. Brown, G. W. Mckinney, M. E. Rising, D. A. Dixon, R. L. Martz, H. G. Hughes, L. J. Cox, A. J. Zukaitis, J. C. Armstrong, R. A. Forster, L. Casswell, *MCNP Version 6.2 Release Notes*, http://doi.org/10.2172/1419730.

[12] https://www.crystals.saint-gobain.com/products/organic-scintillation-materials Accessed: July, 2021

[13] P. L. Feng, J. J. Perry IV, S. Nikodemski, B. W. Jacobs, S. T. Meek, M. D. Allendorf, *J. Am. Chem. Soc*. **2010**,*132*, 15487-15489.

[14] H. Furukawa, N. Ko, Y. B. Go, N. Aratani, S. B. Choi, E. Choi, A. O. Yazaydin, R. Q. Snurr, M. O'Keeffe, J. Kim, O. M. Yaghi, *Science* **2010**, *329*, 424-428

[15] J. J. Perry IV, P. L. Feng, S. T. Meek, K. Leong, F. P. Doty, M. D. Allendorf, *J. Mater. Chem* **2012**, 22, 10235-10248.

[16] M. Fust, H. Kallmann, *Phys. Rev*. **1955**, *97*, 583-587.

[17] R. Zacharia, D. Cossement, L. Lafi, R. Chahine, *J. Mater. Chem.* **2010**, *20* (11), 2145–2151.

[18] a) V. Villemot, M. Hamel, R. B. Pansu, I. Leray, G. H. V. Bertrand, *RSC Adv*. **2020**, 10, 18418-18422 ; b) A. R. Kshirsagar, X. Blase, C. Attaccalite, R. Poloni, *J. Phys. Chem. Lett*. **2021**, *12*, 4045-4051.

[19] M.-M. Bé, V. Chisté, C. Dulieu, M. A. Kellett, X. Mougeot, A. Arinc, V. P. Chechev, N. K. Kuzmenko, T. Kibédi, A. Luca, A. L. Nichols, 2016. Monographie BIPM-5 : Table of Radionucléides. Bureau International des Poids et Mesures. ISBN 978-92- 822-2264-5.

[20] V. I. Tretyak, *Astropart. Phys*. **2010**, *33*, 40-53.

[21] W. W. Moses, G. A. Bizarri, R. T. Williams, S. A. Payne, A. N. Vasil'ev, J. Singh, Q. Li, J. Q. Grim, W.-S. Choong, *IEEE Trans. Nucl. Sci.* **2012**, *59*, 2038-2044.

[22] G. H. V. Bertrand, M. Hamel, S. Normand, F. Sguerra, *Nucl. Instr. Methods A* **2015**, *776*, 114-128.

[23] D. L. Horrocks, *Rev. Sci. Instrum.* **1963**, *34*, 1035-1040.

[24] R. Medishetty, J. K. Zaręba, D. Mayer, M. Samoć, R. A. Fischer, *Chem. Soc. Rev.* **2017**, *46*, 4976-5004.

[25] K. Mitev, C. Dutsov, S. Georgiev, L. Tsankov, T. Boshkova, *IEEE Trans. Nucl. Sci.* **2017**, *64*, 1592-1598.